Neutral and Ionic Metal Methyl Bond Energies: Zn

R. Georgiadis and P. B. Armentrout*[†]

*Contribution from the Chemistry Department, University of California,
Berkeley, California 94720. Received October 16, 1985*

Abstract: Zinc methyl and zinc methyl ion are two competing products studied in the ion beam reactions of Zn^+ with a series of alkanes. While ion beam techniques have long been used to provide bond dissociation energies for ionic transition metal species, including MCH_3^+, this study is one of the first to test the reliability of the technique. In addition, improved instrumentation makes possible the determination of both ionic *and* neutral bond energies. We determine $D°(Zn^+-CH_3) = 3.06 \pm 0.14$ eV (70.6 ± 3.2 kcal/mol) and $D°(Zn-CH_3) = 0.84 \pm 0.14$ eV (19.4 ± 3.2 kcal/mol), both in excellent agreement with the available literature. Coupled with literature thermochemistry, this latter value implies that $D°(CH_3Zn-CH_3) = 69.4 \pm 3.2$ kcal/mol. General features of the reaction cross sections and branching ratios are discussed in terms of a simple qualitative molecular orbital picture.

As work in organometallic and catalytic chemistry increases, so does the need for reliable thermochemical information for organometallic species. While in organic chemistry, a body of thermochemical data has been accumulated that can be used to predict the stability of reactive species and to propose plausible synthetic routes to desired products, a similar body of data does not exist for metal-containing species. To address this deficiency, several methods have been used to measure the strengths of metal–organic ligand bonds. Calorimetric techniques are the most common, although they provide only average bond dissociation energies (BDEs).[1] More useful are individual BDEs for each ligand. Kinetic approaches have been used to estimate individual BDEs, but complications such as competing reactions and secondary reactions limit this potentially general method.[2] Diatomic molecules and a few larger species can be investigated via spectroscopic techniques.[3] Mass spectrometric methods have provided appearance potential,[4] ionization potential,[4] and electron-affinity[5] measurements from which BDEs of certain species can be obtained. Thermal and exothermic reactions of metals and metal compounds have been studied extensively by using high temperature Knudsen cell mass spectrometry.[6] Ion cyclotron resonance mass spectrometry (ICR, FTMS) has been used recently to obtain limits on a number of transition metal ligand BDEs.[7,8]

Another mass spectrometric technique, ion beam mass spectrometry (or ion beam reactive scattering) has recently been utilized for measuring individual BDEs and has provided extensive data on previously unknown systems.[9-11] In this technique, a beam of metal ions of well characterized kinetic energy is collided with a neutral gas, and the ionic products are collected. By varying the interaction energy and determining the energy at which product formation begins, one can obtain the bond strength of the particular ionic species formed. The accuracy of the resulting BDEs and the range of systems reliably investigated have been limited by interpretational and experimental difficulties. There is no generally accepted form for the kinetic-energy dependence

of the cross section for endothermic reactions. This lack of adequate theory makes determination of the experimental thresholds difficult. Several parameterized threshold forms have been used to interpret results,[12] but the experimental data have not allowed a critical evaluation of the different forms. Questions relating to sensitivity, product collection efficiency, energy resolution, and energy calibration have limited the precision and accuracy of the data.

We have addressed the need for improved instrumentation by

(1) Skinner, H. A. *Adv. Organomet. Chem.* **1964**, *2*, 49. Skinner, H. A. *J. Chem. Thermodyn.* **1964**, *10*, 309. Connor, J. A. *Top. Curr. Chem.* **1979**, *71*, 71.

(2) Halpern, J. *Fundamental Research in Homogeneous Catalysis*; Tsutsui, M., Ed.; Plenum Press: New York, 1979; Vol. 3.

(3) Gaydon, A. G. *Dissociation Energies and Spectra of Diatomic Molecules*; Chapman and Hall: London, 1968; Distefano, J. J. *J. Res. Natl. Bur. Stand., Sect. A* **1970**, *74A*, 233. Cheetham, C. J.; Barrow, R. F. *Adv. High Temp. Chem.* **1967**, *1*, 7.

(4) Rosenstock, H. M.; Draxl, K.; Steiner, B. W.; Herron, J. T.; *J. Phys. Chem. Ref. Data Suppl. No. 1* **1977**, *6*.

(5) Stevens, A. E.; Feigerle, C. S.; Lineberger, W. C. *J. Am. Chem. Soc.* **1982**, *104*, 5026–5031. Engelking, P. C.; Lineberger, W. C. *J. Am. Chem. Soc.* **1984**, *106*, 2543–2549.

(6) Gingerich, K. A. *Curr. Top. Mater. Sci.* **1980**, *6*, 345. Gingerich, K. A. *Faraday Symp. Chem. Soc.* **1980**, *14*, 109–125.

(7) Corderman, R. R.; Beauchamp, J. L. *J. Am. Chem. Soc.* **1976**, *98*, 3999. Allison, J.; Ridge, D. P. *Ibid* **1979**, *101*, 4998. Stevens, A. E.; Beauchamp, J. L. *J. Am. Chem. Soc.* **1981**, *103*, 190.

(8) Sallans, L.; Lane, K. R.; Squires, R. R.; Freiser, B. S. *J. Am. Chem. Soc.* **1983**, *105*, 6352–6354. Sallans, L.; Lane, K. R.; Squires, R. R.; Freiser, B. S. *Ibid.* **1985**, *107*, 4379–4385.

(9) Armentrout, P. B.; Beauchamp, J. L. *J. Am. Chem. Soc.* **1980**, *102*, 1736. Armentrout, P. B.; Beauchamp, J. L. *Ibid* **1981**, *103*, 784. Armentrout, P. B.; Halle, L. F.; Beauchamp, J. L. *Ibid* **1981**, *103*, 6501. Halle, L. F.; Armentrout, P. B.; Beauchamp, J. L. *Organometallics* **1982**, *1*, 963.

(10) Mandich, M. L.; Halle, L. F.; Beauchamp, J. L. *J. Am. Chem. Soc.* **1984**, *106*, 4403. Tolbert, M. A.; Beauchamp, J. L. *Ibid* **1984**, *106*, 8117.

(11) Aristov, N.; Armentrout, P. B. *J. Am. Chem. Soc.* **1984**, *106*, 4065. Loh, S. K.; Ervin, K. M.; Armentrout, P. B. *J. Am. Chem. Soc.* **1984**, *106*, 1161. Elkind, J. L.; Armentrout, P. B. *J. Phys. Chem.* **1985**, *89*, 5626–5636.

(12) Armentrout, P. B.; Beauchamp, J. L. *J. Chem. Phys.* **1981**, *74*, 2819–2826.

developing a guided ion beam apparatus[13] which employs an octopole ion trap.[14] This device increases sensitivity, greatly reduces biases introduced by the reaction dynamics, helps insure efficient product collection, and allows accurate calibration of the energy scale. This apparatus has been specifically designed to provide a critical test of the threshold forms. The enhanced sensitivity and collection efficiency allows us to observe slowly rising cross sections and slowly moving products that have not been easily detected before.

In this work the general reactions

$$Zn^+ + CH_3R \rightarrow ZnCH_3^+ + R \qquad (1)$$

$$Zn^+ + CH_3R \rightarrow ZnCH_3 + R^+ \qquad (2)$$

are studied for R = CH_3, C_2H_5, i-C_3H_7, and t-C_4H_9. From the energy dependence of the endothermic reactions, BDEs of product species can be obtained by assuming the absence of activation barriers in excess of the reaction endothermicity, E_0. For reaction 1, the BDE of the metal–alkyl ion, $D^\circ(Zn^+-CH_3)$, is obtained from the simple equation

$$D^\circ(Zn^+-CH_3) = D^\circ(CH_3-R) - E_0 \qquad (3)$$

where $D^\circ(CH_3-R)$ is the BDE of the neutral target molecule. E_0 is determined by measuring the energy threshold for reaction. Neutral BDEs can be obtained from the endothermicity of reaction 2 by using

$$D^\circ(Zn-CH_3) = D^\circ(CH_3-R) - E_0 + IP(R) - IP(Zn) \qquad (4)$$

In previous ion beam studies of other metal systems,[9] only reaction 1 has been studied in detail.

Zinc was chosen for this study because of the availability of reasonably accurate ionic and neutral zinc methyl BDEs from photoionization studies of dimethyl zinc.[15] Thus, this system provides the first rigorous test of the ion beam method as a means of obtaining thermochemical information for *neutral* species and for polyatomic ions. Such a test for diatomic ions, specifically SiH[+], was recently completed in our laboratories.[16] In previous measurements of BDEs using the ion beam method, such a detailed test could not be made since literature values were unknown or had large error limits.

Experimental Section

Details of the guided ion beam apparatus are described elsewhere.[13] Briefly, a beam of ions extracted from an electron impact source is accelerated and focused through a sector magnet. The most abundant zinc isotope, 63.929 u, is selected and then the beam is decelerated to a well-defined kinetic energy and focused into an octopole ion trap. The octopole ion guide passes through a gas cell where the ion beam interacts with the neutral gas molecules under single collision conditions. The ionic products are collected by the octopole trap which insures virtually 100% collection. The product ions and unreacted beam are extracted from the octopole and mass analyzed by a quadrupole mass filter. Their intensities are measured by using a scintillation ion detector and standard ion counting techniques.

Ground state $^2S(3d^{10}4s^1)Zn^+$ ions are produced by electron impact ionization of the metal vapor. Electrons emitted from a tungsten filament are directed through an aperature (2-mm diameter) into a small interaction region (2.5 cm × 1.5 cm) which is maintained at an equipotential. Zinc vapor escaping from a small orifice (0.08-mm diameter) in a resistively heated oven containing zinc metal dust (Mallinckrodt 95.0% pure) is crossed at 90° with an electron beam in the center of the interaction region. The Zn^{+} ions produced are extracted through an aperature (3-mm diameter) in a direction perpendicular to that of the zinc vapor and of the electron beam. The electron energy is set to either 15 or 100 eV. The higher electron energy provides increased Zn^{+} signal, facilitating the experiments. However, under these conditions small exothermic cross sections due to excited state Zn^{+} are observed. Depending on the reaction, the magnitude of the exothermic cross section

ranges from $0.2-2.0 \times 10^{-18}$ cm² at the lowest interaction energies. The percentage of excited state present in the beam produced at 100 eV electron energy cannot be determined absolutely without knowledge of the cross section for reaction. It is estimated to be less than 0.01% by comparison with the calculated magnitude of the collision cross section. At 15 eV electron energy, there is no evidence of the excited state. This is expected since the ionization potential of zinc is 9.458 eV, and the first excited state of Zn^{+} ($3d^{10}4p$) lies 6.01 eV above the ground state.[17] Wherever possible, 100 eV conditions were used to maximize the Zn^{+} beam intensity and thus sensitivity. In most cases, this presents no difficulty since the two states are separated well enough in energy that the ground-state cross section is not obscured by that of the excited state. In cases where this is not true (e.g., neopentane), 15 eV conditions were used.

The translational kinetic energy of the ion beam is directly measured by using the octopole ion trap as a retarding field energy analyzer.[13] Because this energy analysis region is physically the same as the interaction region, ambiguities in the analysis due to contact potentials are eliminated. The nominal ion energy zero is given by the voltage difference applied between the ion source and the DC voltage on the octopole. By scanning through the nominal zero, an energy cutoff curve is obtained and can be numerically differentiated to yield the ion energy distribution. The true energy zero is taken as the peak of the differentiated distribution and can differ from the nominal zero by as much as 0.7 eV. Uncertainties in the absolute energy scale are less than 0.1 eV lab (≤0.03 eV in the center of mass frame (cm) for the ethane system, ≤0.05 eV for the neopentane system). The distribution is nearly Gaussian with widths, FWHM, ranging from 0.15–0.30 eV lab for this ion source (0.05–0.10 eV cm, ethane system; 0.08–0.16 eV, neopentane system). The relative kinetic energy of collision is found by converting the laboratory kinetic energy to the center of mass energy by the equation

$$E = E_{lab} \times M/(M + m) \qquad (5)$$

where m is the mass of zinc, and M is the target molecule mass. At low energies, below ~0.3 eV lab, the center of mass energy is corrected for the ion beam energy distribution as outlined by Ervin and Armentrout.[13]

In these experiments, a large uncertainty in the interaction energy is introduced by the thermal motion of the reactant gas, the so-called Doppler broadening discussed by Chantry.[18] At some relative energy E, this broadening has a width which is approximately

$$FWHM = (11.1\gamma kTE)^{1/2} \qquad (6)$$

where $\gamma = m/(M + m)$, k is the Boltzmann constant, and T is the target gas temperature in Kelvin, here 305 K. This comes to 0.42 eV (cm) for the reaction of Zn^{+} with ethane near threshold ($E \approx 1.0$ eV). Both types of broadening are explicitly included in our analysis of the data by using formula of Lifshitz et al.[19]

The total cross section, σ_{tot}, and the reaction cross section for a specific ionic product, σ_p, are calculated by using eq 7 and 8

$$\sigma_p = \sigma_{tot}(I_p/\Sigma I_p) \qquad (7)$$

$$\sigma_{tot} = \ln [I_r/(I_r + \Sigma I_p)]/nl \qquad (8)$$

where I_r is the transmitted reactant ion beam intensity, I_p is the intensity of a particular product ion, n is the number density of the target gas, and l is the effective length of the gas cell, 8.6 cm. The pressure of the target gas is measured by using an MKS Baratron 310 capacitance manometer. Typically, pressures ranged from 0.02–0.12 mtorr of the neutral gas. This is sufficiently low to ensure that all products are the result of a single bimolecular collision. Absolute cross sections are believed to be accurate within ±20%.[13]

Results

Several endothermic products are observed in the reaction of ground-state Zn^{+} with alkanes. For all the alkanes studied, the major processes are the C–C bond cleavage reactions, formation of $ZnCH_3^+$ and R[+], as shown in reactions 1 and 2. Analogous reactions for C–H bond cleavage, formation of ZnH[+] and RCH_2^+, are also observed for all the alkanes. Also common to all the alkane systems studied are charge-transfer reactions, formation of RCH_3^+. At higher energies, the alkyl ions formed in these reactions are observed to decompose, usually by loss of molecular

(13) Ervin, K, M.; Armentrout, P. B. *J. Chem. Phys.* **1985**, *83*(1), 166–189.

(14) Teloy, E.; Gerlich, D. *Chem. Phys.* **1974**, *4*, 417.

(15) Distefano, G.; Dibeler, V. H. *Int. J. Mass Spectrom. Ion Physics* **1970**, *4*, 59.

(16) Elkind, J. L.; Armentrout, P. B. *J. Phys. Chem.* **1984**, *88*, 5454–5456.

(17) Moore, C. E. *Natl. Stand. Ref. Data Ser. (U.S., Natl. Bur. Stand.)* **35/V.II 1971**.

(18) Chantry, P. J. *J. Chem. Phys.* **1971**, *55*, 2746.

(19) Lifshitz, C.; Wu, R. L. C.; Tiernan, T. O.; Terwilliger, D. T. *J. Chem. Phys.* **1978**, *68*, 247.

Neutral and Ionic Metal Methyl Bond Energies: Zn

J. Am. Chem. Soc., Vol. 108, No. 9, 1986 2121

hydrogen. Only the major product channels, reactions 1 and 2, will be discussed here.

To analyze the data and determine the energy threshold of reaction, E_0, the kinetic energy dependence of reaction cross sections is modeled by using the general form

$$\sigma(E) = \sigma_0(E - E_0)^n/E^m \qquad (9)$$

where σ_0 is an energy independent scaling factor. The exponents, n and m, are tacitly assumed [12] to be related to the number of degrees of freedom in the reactants, transition state, or products and to the dynamics of the reaction. We convolute this form with the energy distributions discussed in the previous section before comparing with the data. The parameters in eq 9 are arbitrarily restricted to integer values of n (when m is held equal to n) and to integer and half-integer values of n and m (when $n \neq m$). Values of n and m ranging from 0–5 were explicitly tested when $n \neq m$ and when $n = m$ values up to 25 were tested. For each trial, one m is set, the other parameters in eq 9 (E_0, σ_0, and n when $n \neq m$) are optimized by using a nonlinear least-squares analysis. The determination of the optimized fit to the data depends on the energy range over which the data and the calculated cross sections are compared. In all the systems studied, for a given energy range, a number of different sets of parameters are found to fit the data with comparable least-squares sums. These fits are visually indistinguishable over the range of energies used in the evaluation. For given values of n and m, the optimum E_0 can be determined to better than 0.05 eV. However, without theoretical guidelines to restrict the values of n and m, the error in the optimum E_0 is given by the range of threshold values found in all the good fits.

Some authors[10,12] have prefered to model the data over all or most of its rising part, i.e, from below the threshold energy to near the maximum in the cross section. While eq 9 is expected to apply to the threshold region, it is not known how high above the threshold it should be applicable. For this reason, we assume in this study that the primary test for a good fit is whether it adequately represents the very onset of the reaction to the degree that our sensitivity allows us to determine it. The onset of the threshold is taken as the region at which the cross section is about twice the magnitude of the background noise (e.g., see the expanded scales in Figures 1–4). We require that the best fit represent the data both at the onset of the threshold and through the largest possible region of the rising data curve. In part because of our very high sensitivity, we have found that it is not always possible to find parameters in eq 9 which allow modeling of the entire rising data curve. In this case, we fit the data over two different energy regions. First, we fit the onset of the threshold and as much of the rising curve as possible. This fit or number of fits represent the data best in the expanded scale. For comparison, a second series of analyses are done on the unexpanded scale, ignoring our additional sensitivity. In this case, we fit essentially all of the rising portion of the cross section but not necessarily the onset of reaction.

Endothermic reaction cross sections generally are observed to increase from threshold, reach a maximum, and then decrease. While such a decrease can be caused by several effects, here, the decrease can be attributed to one of two processes. If another reaction pathway which depletes the precursor to the product under observation becomes available, the cross section for that product will peak near the threshold for this new channel. A more common process is that as the energy is increased the product can be formed with sufficient energy to dissociate. For reaction 1, the thermodynamic threshold for this process, reaction 10,

$$Zn^+ + CH_3R \rightarrow Zn^+ + CH_3 + R \qquad (10)$$
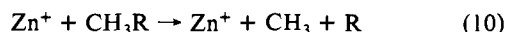
is just the BDE of the neutral reactant. For dissociation to commence at this energy, all excess energy must reside in the Zn^+–CH_3 bond. If the energy is distributed in other degrees of freedom, e.g., relative translation or the internal modes of the neutral product, dissociation will not occur until higher energies. Typically, the cross sections peak near or above the BDE of the neutral reactant and then fall off slowly. This high energy behavior indicates a broad internal energy distribution which has been modeled by using a statistical approach.[12] In the present study,

we use a modified version of this approach which includes angular momentum conservation in the dissociative process. This model, described in detail elsewhere,[20] has two parameters, the onset of the dissociation and the rapidity of the falloff, which are empirically determined.

Zn^+ + Ethane. In this system, the cross section for reaction 1 rises extremely slowly, Figure 1. Expansion of the data by a factor of 100 reveals an apparent threshold about 1 eV lower than that evident in the unexpanded scale. The cross section peaks at about 5 eV, compared to $D°(CH_3–CH_3) = 3.92$ eV. The small exothermic portion seen in the expanded scale of Figure 1a at very low energy is due to a small amount of excited-state Zn^+.

For reaction 1 with ethane, no fit could reproduce both the slow rise, shown in the expanded scale, and the higher cross section behavior above about 3.5 eV or about half the maximum cross section. This may be due to the influence of product dissociation, process 10, which if Doppler broadening is considered may begin as low as 3.0 eV. Therefore, it may not be desirable to fit the rising portion of the curve above this energy. In order to best reproduce the slow rise near threshold, very large values of $n = m$ are required. Parameters for the best fits were integer values of $n = m$ ranging from 15–24. These fits yield E_0 values ranging from 0.8–1.1 eV. The rising portion of the solid line ($n = m = 19$, $E_0 = 0.91$) in Figure 1a is representative of these fits. Other parameters ($n \neq m$) which gave equally good fits are $n = 7.0$, $m = 1.0$, $E_0 = 0.91$; $n = 7.0$, $m = 2.0$, $E_0 = 1.1$ eV; and $n = 8.5$, $m = 4.0$, $E_0 = 1.0$ eV. These fits are required to represent the data well from threshold up to about 3 eV. The best value of E_0 is chosen to be 0.95 ± 0.15 eV, based on the range of fits that best represent the data.

Having found a representative fit to the threshold, the high energy behavior can also be modeled. The fit shown in Figure 1c assumes product dissociation begins at 3.92 eV and was chosen to represent as best as possible both the peak region and falloff after the peak. It is apparent that the model fails to represent the region near the peak adequately but does describe the high energy falloff over an extended 12-eV range.

If we treat the data on the unexpanded scale as if our sensitivity were low, then we find that the best fit for the overall cross section, fitting up to $\simeq 3.5$ eV, is $n = m = 3$, $E_0 = 2.17$ eV. This is about 1.2 eV higher than the threshold determined if the slow rise is included in the fitting. Using these parameters and fitting at high energy gives a curve which more closely represents the peak shape of the cross section than the fit shown in Figure 1c.

The cross section for reaction 2, Figure 1b, is about an order of magnitude smaller than process 1 and behaves very differently. It rises to a maximum at about 6 eV and then stays fairly constant, as shown in Figure 1c. This is presumably because no low energy dissociation channels are available to this product ion. The threshold behavior for the CH_3^+ product does not have the slow rising behavior seen with $ZnCH_3^+$. The cross section from the onset up to the peak is represented well by eq 9 by using parameters that range from $n = m = 6$, $E_0 = 3.38$ eV to $n = m = 4$, $E_0 = 3.71$ eV. This good agreement obtains despite the fact that the fitting range is only up to 4.30 eV. The best value for E_0 is 3.54 ± 0.17 eV. A representative fit ($n = m = 5$, $E_0 = 3.46$ eV) which includes high energy modeling up to 6 eV is shown in Figure 1b. Large values of $n = m$ do not adequately fit the data. Note that at threshold the neutral product accompanying CH_3^+ formation must be $ZnCH_3$, as reaction 11 cannot occur until 4.30

$$Zn^+ + RCH_3 \rightarrow Zn + R^+ + CH_3 \qquad (11)$$

eV. At much higher energies ($\sim$9 eV) the formation of other accompanying neutral products becomes energetically feasible and may contribute to the observed cross section.

Zn^+ + Propane. The cross section for reaction 1 with propane also shows somewhat slow-rising behavior, Figure 2a. The curve peaks between 4 and 5 eV, consistent with the $D°(CH_3–C_2H_5)$ of 3.72 eV. As before, the best fits require large values of $n =$

(20) Weber, M. E.; Elkind, J. L.; Armentrout, P. B. *J. Chem. Phys.* **1986**, *84*, 1521–1529.

2122 *J. Am. Chem. Soc., Vol. 108, No. 9, 1986*

Georgiadis and Armentrout
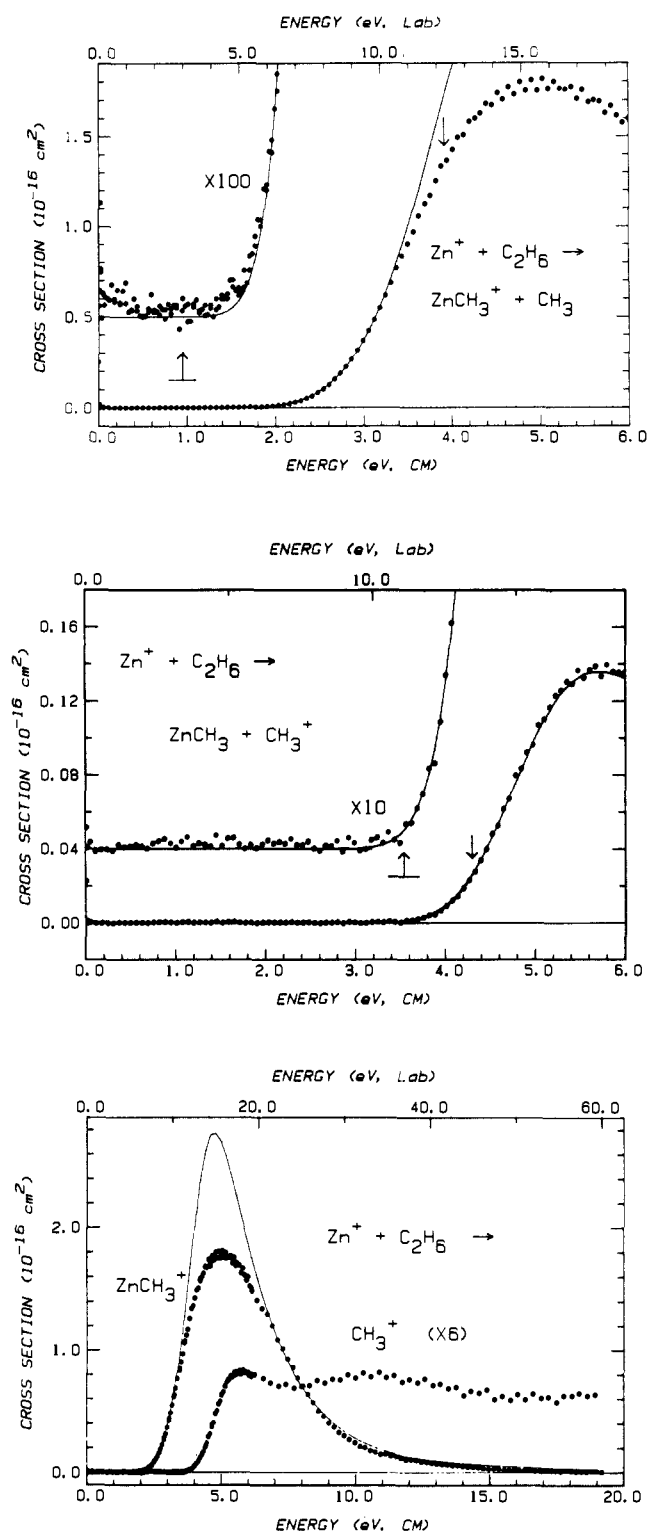
Figure 1. Cross sections for reaction 1, part a, and reaction 2, part b, with R = CH₃ (ethane system) as a function of kinetic energy in the center of mass frame (lower x-axis) and laboratory frame (upper x-axis). The data are also shown on an expanded scale with the zero offset for clarity. For Figure 1a, an additional data set is also plotted on the expanded scale. Solid lines are representative best fits to the data using eq 9 (see Discussion in text). In both part a and part b, the arrow at low energy shows the position of our best determination of the threshold energy E_0 and the error associated with this value. In part a, the arrow at higher energy shows the threshold for product dissociation, reaction 10. In part b, the arrow at higher energy shows the threshold for reaction 11. Part c shows the data extended to higher energies. That shown for CH₃⁺ is the average of several data files and has been expanded by a factor of 6. The data plotted in a and b, extending to 6 eV, are also shown in part c.
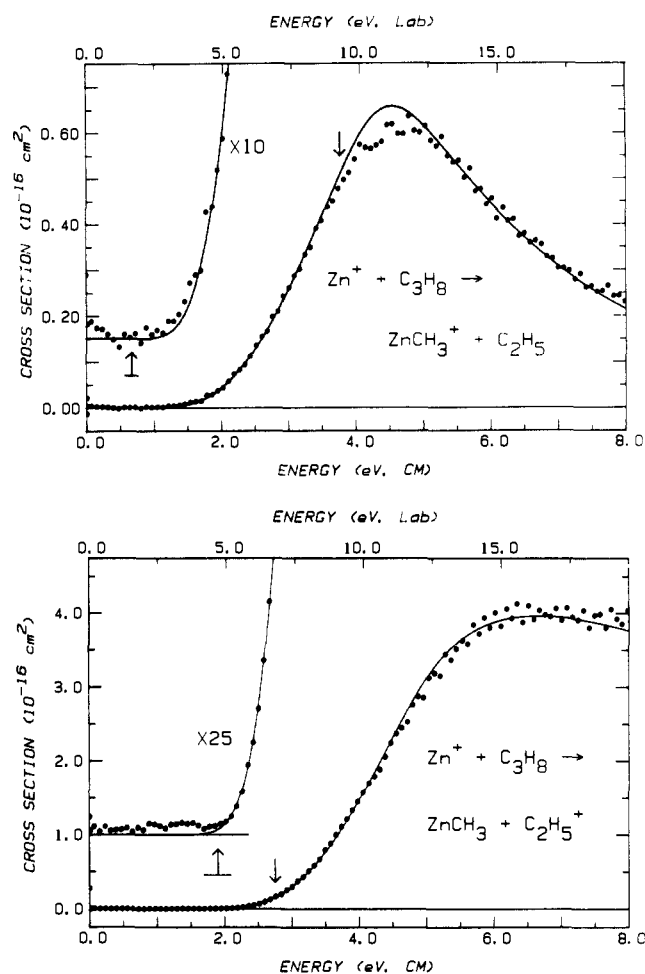
Figure 2. Cross sections for reaction 1, part a, and reaction 2, part b, with R = C₂H₅ (propane system) as a function of kinetic energy in the center of mass frame (lower axis) and laboratory frame (upper axis). The data are also shown on an expanded scale with the zero offset for clarity. Solid lines are the representative best fits to the data using eq 9 (see Discussion in text). In both part a and part b, the arrow at low energy shows the position of our best determination of the threshold energy E_0 and the error associated with this value. In part a, the arrow at higher energy shows the threshold for product dissociation, reaction 10. In part b, the arrow at higher energy shows the threshold for reaction 11.

m. In this case, integer values of $n = m$ ranging from 10–15 give the best fit to the data over the range of the threshold onset to 3.5 eV. These yield a range of values for E_0 of 0.58–0.78 eV. The best value of the threshold is chosen to be 0.68 ± 0.10 eV. A representative fit ($n = m = 11$, $E_0 = 0.71$ eV) is shown in Figure 2a. This includes high energy modeling with product dissociation beginning at 3.83 eV. By treating the data on the unexpanded scale and fitting the overall shape of the curve but not the slow rise, we find that $n = m = 3$, $E_0 = 1.60$ eV and $n = m = 5$, $E_0 = 1.20$ eV can represent the cross section well.

The cross section for reaction 2 with propane, Figure 2b, resembles that of ethane except that it is much larger relative to the cross section of reaction 1. The curve peaks at about 6 eV and remains high for several eV before falling off. The curve from onset to 4.5 eV is fit with low values of $n = m$. The best fits range from $n = m = 4$, $E_0 = 2.1$ eV to $n = m = 6$, $E_0 = 1.71$ eV yielding a threshold of 1.91 ± 0.20 eV. High values of $n = m$ do not adequately fit the data. A representative fit ($n = m = 5$, $E_0 = 1.90$ eV) including high energy modeling is shown in Figure 2b. Note that process 11 cannot begin until 2.76 eV.

Zn⁺ + Isobutane. In contrast with the other two systems, reaction 1 with R = isopropyl has a fairly steep rise, Figure 3a. The curve peaks between 3 and 4 eV, lower in energy relative to the neutral BDE than seen for the ethane or propane systems, and $D°(CH_3-i-C_3H_7) = 3.79$ eV. At high energies, a much slower
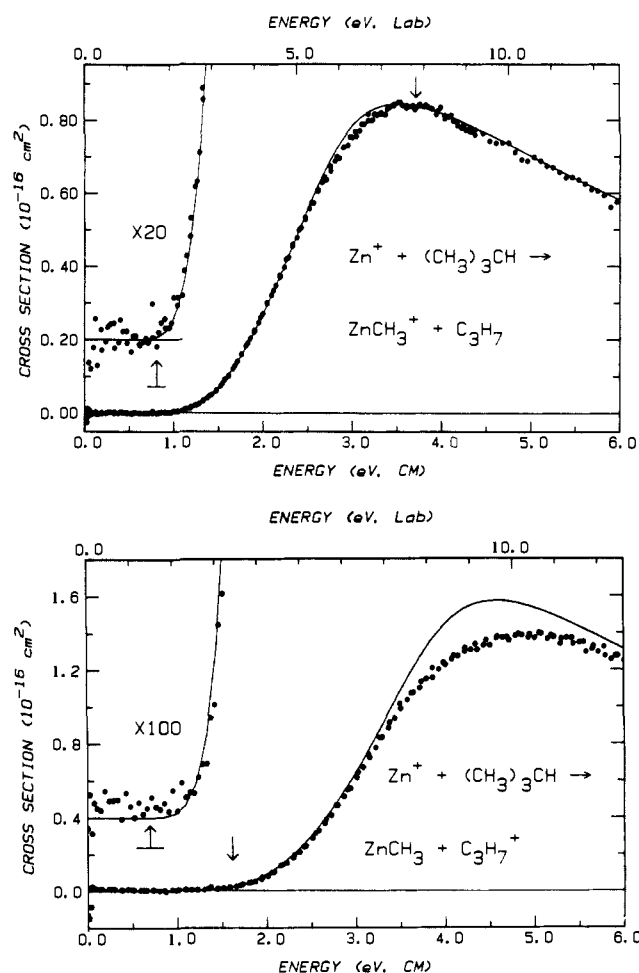
Figure 3. Same as Figure 2 with R = $(CH_3)_2CH$ (isobutane system).

Figure 4. Same as Figure 2 with R = $(CH_3)_3C$ (neopentane system).

falloff is seen in this cross section than in the two previous cases for the same product. Values of $n = m$ ranging from 5–8 provide the best fit to the data up to 2.6 eV. The corresponding E_0 values range from 0.71–0.91 eV, yielding a best E_0 value of 0.81 ± 0.10 eV. The fit shown in Figure 3a ($n = m = 6$, $E_0 = 0.83$ eV) is representative. To model the high energy behavior it had to be assumed that the onset of product dissociation begins about 1.0 eV lower than the neutral BDE.

Unlike the previous two cases, there are no other smaller values of $n = m$ that represent the unexpanded data. Here, the fits that best represent the onset of the threshold also reproduce the entire curve, if dissociation is assumed to begin early.

The product for reaction 2 with R = isopropyl, Figure 3b, does not rise steeply as we saw in the ethane and propane systems. The cross section for $C_3H_7^+$ shows a slow rise and is fit with large values of $n = m$ up to 3.26 eV. The best fits range from $n = m = 18$, $E_0 = 0.55$ eV to $n = m = 10$, $E_0 = 0.85$ eV, yielding a threshold of $E_0 = 0.70 \pm 0.15$ eV. A representative fit ($n = m = 13$, $E_0 = 0.71$ eV) is shown in Figure 3b. We find that these parameters do not represent the peak region well in the high energy modeling. This was also seen in Figure 1a where similarly high values of n and m are required to reproduce the slow rise. If the data are fit with emphasis on the overall shape of the curve on the unexpanded scale, we find that the best fit is given by $n = m = 5$, $E_0 = 1.25$ eV. Reaction 11 cannot begin until 1.62 eV.

Zn^+ + Neopentane. For reaction 1 with R = *tert*-butyl, Figure 4a, the cross section for $ZnCH_3^+$ rises slowly in the threshold region and continues to rise well past the dissociation energy for the neutral reactant, 3.69 eV. This may not be surprising considering the many degrees of freedom in the neutral product formed in reaction 1 in this case. However, this trend was not observed in the reaction of isobutane where the $ZnCH_3^+$ product was observed to peak early rather than late. The cross section for this process is not well represented by eq 9 when n is restricted
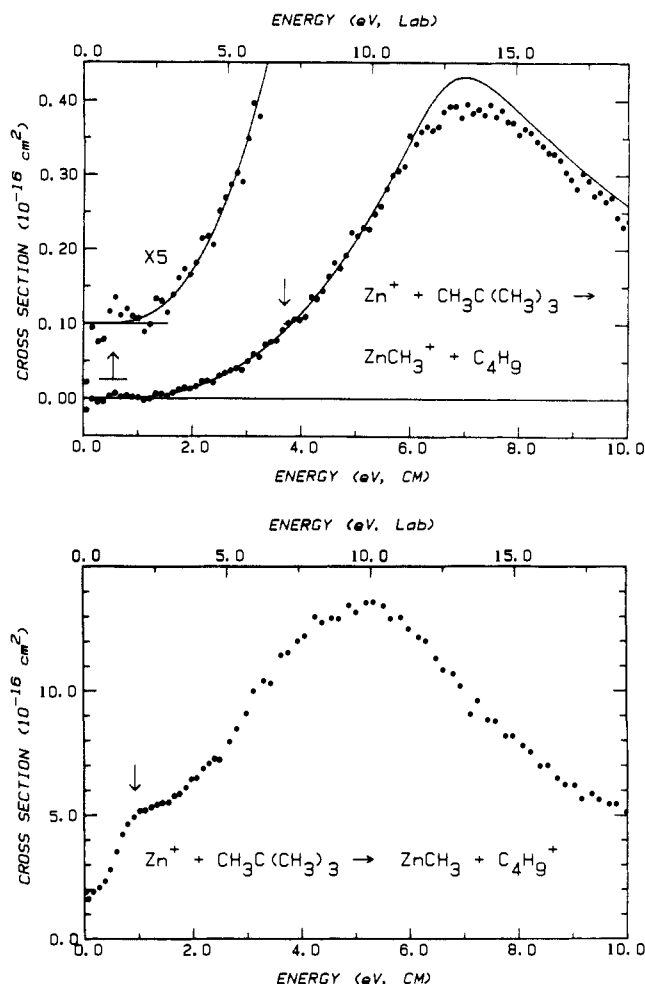
to be equal to m. Various other fits ($n \neq m$) reproduce the entire curve from onset to high energy yielding values of E_0 from 0.3 eV–0.8 eV. The best fit, over a range of energies up to 3.55 eV, is $n = 2.5$, $m = 0$, $E_0 = 0.50$ eV, Figure 4a. Based on the center of the range of good fits, the optimum E_0 is chosen to be 0.55 ± 0.25 eV.

Reaction 2 for neopentane, Figure 4b, has quite different behavior from all the previous products. The cross section appears to be endothermic, rises sharply, then peaks about 5 eV and finally begins to falloff at higher energies. However, the cross section is nonzero even at the lowest energies we can obtain. We have verified that the nonzero cross section is not due to excited state Zn^+ and speculate that it is due to thermally excited C_5H_{12}. Reaction 11 has an onset at about 0.93 eV. The shape of the cross section in that energy region is consistent with a new channel becoming available at about 1 eV. The cross section at the lowest energies cannot be fit with eq 9 to yield a reliable value of E_0. The threshold is estimated by inspection to be ≤0.20 eV.

Discussion

Thermochemistry. The endothermicities of reactions 1 and 2 for the four alkane systems may be used to calculate $D°(ZnCH_3^+)$ and $D°(ZnCH_3)$ provided that the thermochemistry for Zn^+, Zn, CH_3R, R^+, and R is known. Table I lists the literature data needed. We obtain the following range of values for $D°(ZnCH_3^+)$: 2.97 ± 0.15, 3.15 ± 0.10, 2.98 ± 0.10, and 3.14 ± 0.25 eV for the ethane, propane, isobutane, and neopentane systems, respectively. Despite the different threshold behavior exhibited in each case, these results are remarkably consistent within experimental error. The average value with pooled estimate of error is 3.06 ± 0.14 eV (70.6 ± 3.2 kcal/mol), which we take as our best value for $D°(Zn^+-CH_3)$.

In order to make an assessment of the accuracy of the beam method, we compare these results to literature values. A pho-

2124 *J. Am. Chem. Soc., Vol. 108, No. 9, 1986*

Georgiadis and Armentrout

Table I. Thermochemical Data at 298 K[a]

X	$\Delta H_f°(X)$ (kcal/mol)	$\Delta H_f°(X^+)$ (kcal/mol)
CH_3	35.1 (0.5)	262.0 (1.0)
C_2H_5	28.3 (1.1)	221.8 (1.1)
C_2H_6	-20.24 (0.10)	
$(CH_3)_2CH$	20.0 (1.1)	187.9 (1.1)
C_3H_8	-24.82 (0.14)	
$C(CH_3)_3$	10.3 (1.2)	164.8
$CH(CH_3)_3$	-32.4 (0.13)	
$C(CH_3)_4$	-39.67 (0.1)	
Zn	31.245[b]	249.36[b]
$ZnCH_3$	24.6 (2)[c]	213.3 (0.7)[d]
	31.6 (4)[e]	
	43.6 (4)[f]	
	45.6 (4)[g]	
	46.9 (3.2)[h]	213.9 (3.2)[h]
$Zn(CH_3)_2$	12.67 (0.08)[b]	221.7 (0.8)[b]

[a]Numbers in parentheses are the error associated with the values. Alkane heats of formation are from Cox, J. D.; Pilcher, G. *Thermochemistry of Organic and Organometallic Compounds*; Academic Press: New York, 1970 and alkyl radical and ion heats of formation are from Schultz, J. C.; Houle, F. A.; Beauchamp, J. L. *J. Am. Chem. Soc.* **1984**, *106*, 3917-3927. [b]From Wagman, D. D. et al. *J. Chem. Ref. Data Suppl. No. 2* **1982**, *11*. [c]Calculated by using the $D°$-(CH_3Zn-CH_3) = 47 ± 2 kcal/mol, ref 15, and other data in Table I. [d]Calculated by using the AP $(ZnCH_3^+, Zn(CH_3)_2)$ = 10.22 ± 0.02 eV, ref 15, and other data in Table I. [e]Reference 20. [f]Reference 21. [g]Reference 22. [h]Present work.

toionization study of dimethyl zinc[15] provides an appearance potential for $ZnCH_3^+$ (AP = 10.22 ± 0.02 eV), from which a value for $\Delta H_f°(ZnCH_3^+)$ of 215.2 ± 0.5 kcal/ mol was reported based on a calculation using $\Delta H_f°(CH_3)$ = 33.2 kcal/mol and $\Delta H_f°$-$(Zn(CH_3)_2)$ = 12.67 kcal/mol. This value leads to the reported[10] value for $D°(Zn^+-CH_3)$ of 67 ± 1 kcal/mol. A recalculation which uses the more recent thermochemical data from Table I yields $\Delta H_f°(ZnCH_3^+)$ = 213.3 ± 0.7 kcal/mol and $D°(Zn^+-CH_3)$ = 71.2 ± 0.9 kcal/mol, in excellent agreement with our value.

From reaction 2, the range of values for $D°(Zn-CH_3)$ is found to be 0.76 ± 0.17, 0.85 ± 0.18, and 0.92 ± 0.10 eV, for the first three alkanes. These values average to 0.84 ± 0.14 eV (19.4 ± 3.2 kcal/mol), which is our best experimental value for $D°(Zn-CH_3)$. This value is consistent with our results for neopentane which place an upper limit on $D°(Zn-CH_3)$ of 0.93 eV (21.5 kcal/mol) based on the fact that reaction 2 is endothermic and a lower limit of 0.73 eV (16.8 kcal/mol) based on an estimated endothermicity of ≤0.2 eV.

The BDE of neutral $ZnCH_3$ is less accurately known. From Table I, the sum of the first and second bond energies in $Zn(CH_3)_2$ is 88.8 ± 0.8 kcal/mol. To find $D°(Zn-CH_3)$, $D°(CH_3Zn-CH_3)$ is required. Three early results of this BDE are centered on a value of 47 ± 2 kcal/mol.[15] In 1970, new experimental results[21] yielded 54 kcal/mol, but a reinterpretation of these results suggested 66 kcal/mol instead.[22] Critical evaluation of the literature[23] (which includes this reevaluated value) places the value of $D°$-(CH_3Zn-CH_3) at 68 ± 4 kcal/mol which yields $D°(Zn-CH_3)$ = 21 ± 4 kcal/mol. The result obtained here strongly supports only the latter value. Note also that the value $D°(CH_3Zn-CH_3)$ = 69.4 ± 3.2 kcal/mol can be derived from our results.

Had we considered only the unexpanded scale and emphasized fitting the entire curves, we would have obtained the following results for the first three alkane systems: $D°(Zn^+-CH_3)$ = 1.75 ± 0.20, 2.43 ± 0.20, and 2.98 ± 0.10 eV. It is obvious that these results represent lower limits to the true BDEs, since the interpreted thresholds represent upper limits to the true E_0. From these results, it would have been difficult to determine a BDE with any degree of reliability. We could have said only that $D°(Zn^+-CH_3)$ ≥ 2.98 eV. Similarly for the neutral BDE results, we would have

(21) Dunlop, A. N.; Price, S. J. W. *Can. J. Chem.* **1970**, *48*, 3205.

(22) From Smith and Patrick (Smith, G. P.; Patrick, R. *Int. J. Chem. Kin.* **1983**, *15*, 167) based on reevaluation of the data of ref 21.

(23) McMillan, D. F.; Golden, D. M. *Ann. Rev. Phys. Chem.* **1982**, *33*, 493-532.

Table II. Molecular Orbital Energies

species	MO energy[a] (eV)	symbol[b]
C_2H_6	-11.52[c]	$\sigma(RM)$
	15.55[d]	$\sigma^*(RM)$
C_3H_8	-10.94[c]	$\sigma(RM)$
	17.22[d]	$\sigma^*(RM)$
C_4H_{10}	-10.57[c]	$\sigma(RM)$
	18[e]	$\sigma^*(RM)$
C_5H_{12}	-10.35[c]	$\sigma(RM)$
	18[e]	$\sigma^*(RM)$
Zn	-9.458	4s Zn
CH_3	-9.81	$n(R)$
C_2H_5	-8.38	$n(R)$
C_3H_7	-7.36	$n(R)$
C_4H_9	-6.70	$n(R)$
$ZnCH_3$	-7.33	$\sigma^*(ZnM)$
	-13[e]	$\sigma(ZnM)$

[a]Koopmans' theorem prediction (see Koopmans, T. C.; *Physica* **1933**, *1*, 104 (negative IP = orbital energy from which the electron is removed). Calculated by using data in Table I except as noted. [b]Symbols used in Figure 5 to label the orbital. See discussion in text. [c]Rosenstock, H. M. et al. *J. Chem. Phys. Ref. Data Suppl. No. 1* **1977**, *6*. [d]Jorgensen, W. L.; Salem, L. *The Organic Chemist's Book of Orbitals*; Academic Press: New York, 1973. [e]Estimated value.
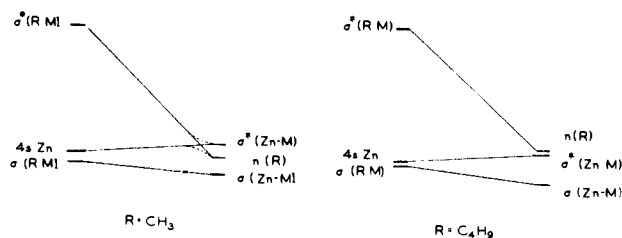
Figure 5. Qualitative molecular orbital correlation diagrams for reactions 1 and 2. Orbital energies (along the y-axis) indicated by horizontal lines are given in Table II. Solid lines show diabatic correlations among these while dashed lines indicate adiabatic correlations. The orbital energies shown in part a are appropriate for R = CH_3 (ethane system). The relative ordering for R = C_2H_5 (propane system) is the same. Part b shows orbital energies appropriate for R = C_4H_9 (neopentane system).

obtained values for $D°(Zn-CH_3)$ of 0.80 ± 0.17, 0.81 ± 0.18, and 0.54 ± 0.20 eV. Again, the results are not consistent except as lower limits to the true BDE.

Molecular Orbital Correlations. Our results show the competition between reaction 1 and 2, which can be thought of simply as the competition between $ZnCH_3^+$ and R^+ for the odd electron. As R^+ varies from methyl to *tert*-butyl, reaction 2 becomes energetically more favorable. This is reflected in the ionization potentials of $ZnCH_3$· and R·, since $IP(CH_3)$ > $IP(C_2H_5)$ > IP-(C_3H_7) ≈ $IP(ZnCH_3)$ > $IP(C_4H_9)$, Table II. For ethane and propane, reaction 1 is clearly favored thermodynamically by 2.59 ± 0.17 and 1.23 ± 0.20 eV, respectively. For isobutane, there is some uncertainty, while for neopentane, reaction 2 is favored by at least 0.35 ± 0.25 eV. Our results are consistent with the predictions that can be made with available thermochemistry, within experimental error. In order to interpret features of the cross sections such as the slope near threshold and the height and position of the peak, a more detailed picture of the reaction is required.

Molecular orbital correlation diagrams have been used for ion molecule reactions to explain the reaction dynamics of simple systems involving three or four atoms.[24] Although the reactions considered here are much more complicated, several simplifying assumptions allow construction of an MO correlation diagram which illustrates the dominant effects as reactants evolve to products. For the Zn^+ reactant, we assume that the filled 3d shell is unavailable for bonding. Consequently, the 4s orbital is the dominant bonding orbital on the Zn. For the alkane reactant,

(24) Mahan, B. H. *J. Chem. Phys.* **1971**, *55*(3), 1436 and references therein.

the only electrons involved in either process 1 or 2 are the two electrons in the C–C bond cleaved during reaction. To a good approximation, therefore, the other molecular orbitals of the methyl (M) and alkyl (R) can be neglected. Nominally, M and R are then treated as one electron atoms. The result is that the reactions of interest here can be viewed as simple three-electron systems, a problem which has been discussed extensively in the literature.[24]

In analogy with such discussions and using the orbital energies given in Table II, the diagrams shown in Figure 5 can be drawn. On the reactant side, there are three orbitals of interest. The lowest is the doubly occupied bonding orbital $\sigma(RM)$ of the alkane, followed by the singly occupied 4s orbital on the Zn and the unoccupied R–M antibonding orbital, $\sigma^*(RM)$. Since the energies of $\sigma(RM)$ and $\sigma^*(RM)$ are not very sensitive to the identity of R, Table II, the ordering of these three reactant orbitals is the same for all four alkane systems under consideration. On the products side, the lowest energy orbital is presumed to be the Zn–M bonding orbital, $\sigma(ZnM)$. While the energy of this orbital is not known, it almost certainly lies below the other product orbitals. It has been estimated as –13 eV, about two $Zn^+ - CH_3$ bond energies, below $\sigma^*(ZnM)$. Any uncertainty in its exact position is unlikely to affect the qualitative conclusions of the resulting MO diagram. The energy of the ZnM antibonding orbital, $\sigma^*(ZnM)$, is taken as the ionization potential (IP) of neutral $ZnCH_3$. Likewise the third product orbital, the radical alkyl orbital of R, $n(R)$, is assigned an energy corresponding to its IP, Table II. Obviously, the energies of $\sigma(ZnM)$ and $\sigma^*(ZnM)$ do not change with R, but the energy of $n(R)$ varies substantially. Two general situations can result. If IP(R) > IP($ZnCH_3$), as in the ethane and propane systems, the MO diagram looks like Figure 5a. (Note the orbital energies are the negative of the IP's.) If IP(R) < IP($ZnCH_3$), as for neopentane, then the MO diagram shown in Figure 5b is obtained. The isobutane system represents an intermediate case where the IP's are nearly equivalent.

Having ascertained the ordering of the salient MO's, we now determine the correlation between the reactant and product orbitals. Literature discussions of analogous three-atom systems[24] utilize the nodal structure of the evolving MO's to determine these correlations. Such considerations show that $\sigma(RM)$ correlates with $\sigma(ZnM)$, 4s(Zn) correlates with $\sigma^*(ZnM)$, and $\sigma^*(RM)$ correlates with $n(R)$, Figure 5. These correlations are independent of the overall symmetry of the reaction, i.e., whether Zn^+ approaches RM end-on or side-on, given the assumption of the three-electron system. Note that in Figure 5a the correlations for the upper two MO's cross. This crossing will be avoided, as indicated by the dashed lines, in all interaction geometries.[25] In the discussion below, we refer to the full lines of Figure 5 as diabatic correlations, while the dashed lines (if present) are adiabatic correlations.

Finally, consider the electron occupation of the MO diagram for the reactions of interest. For ethane, R = CH_3, the situation in Figure 5a holds. The two electrons which begin in $\sigma(RM)$ flow into $\sigma(ZnM)$ as required for both reactions 1 and 2. The electron in the 4s(Zn) adiabatically evolves to the $n(R)$. This corresponds to reaction 1. In order for reaction 2 to occur, the reaction must proceed along the diabatic correlations. A similar situation holds for reaction with propane. Experimentally, reaction 1 is the thermodynamically favored process for both systems. This adiabatic channel has slowly rising threshold behavior. The cross section for reaction 2, the diabatic channel, rises steeply once energetically feasible.

For neopentane, the MO diagram shown in Figure 5b is appropriate. Reaction 2 is both the adiabatically and diabatically favored channel. This is reflected in the cross section for formation of $C_4H_9^+$ which rises steeply and reaches a fairly large magnitude. According to the MO diagram 5b, reaction 1 is now inaccessible.

This seems consistent with the experimental evidence as the cross section is quite small for $ZnCH_3^+$ and rises very slowly. That reaction 1 occurs at all implies that the potential energy surfaces for process 1 and 2 do mix. One possible mechanism for this involves formation of a long-lived complex, in which electron reorganization may occur.

For isobutane, the orbital energies of $n(R)$ and $\sigma^*(ZnM)$ are nearly degenerate. Thus, it is unclear whether the most appropriate MO correlation diagram is that of Figure 5, a or b. Experimentally, we find this system is quite different from the others. Now, the cross section for $C_3H_7^+$ rises slowly in the threshold while that for $ZnCH_3^+$ has a rather steep onset. This relatively odd behavior may be the result of extensive interactions between the two product channels due to the near energetic resonance. This is consistent with the observation that the $ZnCH_3^+$ cross section peaks are below the energy required for dissociation, in marked contrast to the behavior observed in the other systems. This early peaking cross section can only be the result of strong competition with another reaction, persumably reaction 2. Early peaking behavior dominates this system despite the fact that the neutral product can carry away almost as much energy here as in the neopentane system, where late-peaking behavior is seen.

In general, we observe that cross sections for diabatically allowed processes rise sharply from threshold. The competing adiabatic channel cross section rises slowly, as in the cases of ethane and propane. The isobutane system does not seem to follow these patterns, which we attribute to the very strong competition between the two processes. The diabatic channel, reaction 2, generally has a larger cross section than reaction 1 unless the latter is *strongly* favored by thermodynamics, as in the case of CH_3^+ in the ethane system. Formation of this product is 2.59 eV more endothermic than that of the $ZnCH_3^+$ product. The diabatic channels are presumably favored by direct mechanisms of reaction where there is no electronic reorganization, i.e., coupling between two potential energy surfaces. The adiabatic channels may be accessed by low-energy collisions and should be enhanced by the formation of long-lived intermediates. This maximizes the probability of electron reorganization. Although the nature of the intermediate is not known, the data in Table I show that Zn^+ insertion into the C–C bond of ethane to form $Zn(CH_3)_2^+$ is exothermic by 7.4 kcal/mol. Therefore, a strongly bound intermediate is not expected, which is consistent with the dominance of diabatic behavior in the experiments. However, the fact that a well exists on the PES may provide a means for coupling surfaces as suggested for the neopentane system.

Other Metal Systems. Previously published reports of ion-beam studies of transition-metal ions reacting with alkanes have provided thermochemical data for several metal–methyl ions.[9,10,27] The interpretation of the data differs markedly from this work. Analysis of endothermic-reaction cross sections has relied heavily on the high-energy behavior to restrict the range of parameters used in eq 9.[12] Especially where sensitivity is low, good fits have been judged on the basis of reproducing the entire cross section curve. As we have shown, this interpretation for the zinc system leads to upper bounds to the threshold.

The proper analysis for this system is with emphasis on the threshold region. This is the first time that slowly rising cross sections have been observed for metal-ion reactions with alkanes, and as a consequence the first time such large values of $n = m$ have been used to represent the data. Such behavior is not general, however, as evidenced by a comparison between this work and previous ion-beam studies of Sc^+, Ti^+, V^+, Fe^+, Co^+, and Ni^+.[9,10,27] Reactions of V^+ with ethane, ethylene, and acetylene[26] are representative of these systems and provide data of comparable quality to that described here for Zn^+. The major endothermic process in the reaction of ground state V^+ with ethane is formation of VCH_3^+, analogous to process 1. It does not show slow-rising behavior in the threshold region. Further differences in the reactivity of V^+ with ethane include the observation of products such

---

(25) The only possible exception is in the case of ethane where it is possible to maintain C_{2v} symmetry throughout the course of the reaction. In this symmetry, the crossing will not be avoided. Such a constrained reaction geometry is highly unlikely.

(26) Aristov, N.; Armentrout, P. B. *J. Am. Chem. Soc.*, in press.
(27) Aristov, N.; Armentrout, P. B., unpublished work.

as VC$^+$, VCH$^+$, and VCH$_2^+$ which are not seen with zinc. Similar reactivity is observed for reactions of vanadium ions with other alkanes.[27] Conversely, reaction 2 is not observed for the reaction of vanadium ions with ethane and propane. For the isobutane and neopentane systems, this process is observed although it is small relative to the competing VCH$_3^+$ channel.

There are many dissimilarities between V$^+$ and Zn$^+$ which may account for their different reactivity. At first glance, one of the striking differences is that vanadium has a much lower ionization potential (6.74 eV) than zinc (9.458 eV). Considering only the reactant molecular orbitals analogous to those shown in Figure 5, the difference in the orbital energy (IP) of the metal ions does not change the *relative* ordering of the orbitals. Thus, the lower ionization potential of vanadium should not affect the qualitative correlations.

The most important consideration is electronic structure. The ground state of Zn$^+$ is ^{2}S (3d^{10}4s^1) while for V$^+$ it is ^{5}D (3d^4). If we were to consider only the 4s orbital from the vanadium ion, the orbital correlations would be the same as in the zinc system. Mixing of the filled σ_{RM} and the now empty 4s of V$^+$ would occur. The *diabatic* path would still be the formation of R$^+$, for both the vanadium and the zinc system, in this simplistic MO approach. But the d orbitals must be considered in the vanadium case, and this complicates the molecular correlation picture. Depending on the symmetry, some of the d orbitals will remain unperturbed and nonbonding, while others will be involved in avoided crossings in the MO correlation diagram. The adiabatic pathway will involve many more crossings for the vanadium system compared with zinc.

The reactions of vanadium ions with various hydrocarbons have been interpreted based on the assumption that the reaction pro-

ceeds by metal-ion insertion into C–C or C–H bonds.[26] Formation of such an intermediate complex would be facilitated by the availability of empty d orbitals and would allow electronic reorganization to occur. This is consistent with the dominance of the adiabatic processes in the reactions of V$^+$ with alkanes. Similar considerations presumably hold for Sc$^+$, Ti$^+$, Fe$^+$, Co$^+$, and Ni$^+$.

Preliminary results for the reactions of two other s^1 ions, Ca$^+$ (4s^1) and Mn$^+$ (3d^{5}4s^1), with ethane have been examined for slow rising threshold behavior and for the presence of reaction 2. Neither is observed in the Ca$^+$ system. Although not a transition metal, it is possible that the empty d orbitals on Ca$^+$ contribute to its bonding, much like the vanadium system. For Mn$^+$, reaction 2 is not observed. Reaction 1 is observed but the existence of a small amount (<0.2%) of a low-lying excited state of Mn$^+$ in the reactant beam makes the interpretion difficult. The apparent threshold for ground-state Mn$^+$ is definitely greater than the thermodynamic value, and the position of the peak cross section for reaction 1 is unusually high in energy. These observations are consistent either with slow rising threshold behavior or a barrier to the reaction or both. Preliminary data from reaction 1 for Mn$^+$ with neopentane are consistent with the slow rising threshold interpretation of the ethane data. Thus while the cross section behavior found in this study for Zn$^+$ is not completely general, indications are that it is representative of a class of systems.

Laser Spectroscopy of Alkaline Earth Monoalkoxide Free Radicals

C. R. Brazier, L. C. Ellingboe, S. Kinsey-Nielsen, and P. F. Bernath*

Contribution from the Department of Chemistry, University of Arizona, Tucson, Arizona 85721. Received August 6, 1985

Abstract: We have observed a new class of organometallic free radicals. The reaction of the alkaline earth metals Ca, Sr, and Ba in the vapor phase with the alcohols methanol, ethanol, propanol, and butanol yields the metal monoalkoxides. The species are all locally linear near the metal and exhibit characteristic spin–orbit splittings in the $\tilde{A}^2\Pi$ state. The vibrational frequencies are interpreted and possible reaction mechanisms suggested.

The inteaction of metals with organic molecules is one of the principal themes of modern chemistry. Recently, we have discovered a large number of new gas-phase organometallic free radicals[1] produced by the reaction of Ca, Sr, and Ba vapors with alcohols, aldehydes, ketones, thioethers,[2] isocyanic acid,[3] and carboxylic acids.[4] In this paper we report on the alkaline earth monoalkoxide radicals.

The smallest members of the alkaline earth alkoxide (M–O–R; M = Mg, Ca, Sr, and Ba) series are the triatomic monohydroxides (R = H). The alkaline earth monohydroxide radicals commonly

occur in flames containing traces of alkaline earth salts.[5] The flame observations date back to the work of Herschel[6] in 1823, although it was not until 1955 that James and Sugden[7] correctly assigned the carrier of the emission to the alkaline earth monohydroxides. ESR spectra of matrix-isolated BeOH[8] and MgOH[9] suggested that, like the alkali hydroxides, the alkaline earth hydroxides are linear. (Although MgOH has a bent excited state.[10]) More recently infrared spectra of matrix-isolated SrOH and BaOH were observed by Kauffman, Hauge, and Margrave.[11]

(1) Brazier, C. R.; Bernath, P. F.; Kinsey-Nielsen, S.; Ellingboe, L. C. *J. Chem. Phys.* **1985**, *82*, 1043–1045.

(2) Ram, R. S.; Brazier, C. R.; Bernath, P. F., unpublished results.

(3) Ellingboe, L. C.; Bopegedera, A. M. R. P.; Brazier, C. R.; Bernath, P. F. *Chem. Phys. Lett.*, in press.

(4) Brazier, C. R.; Ellingboe, L. C.; Kinsey-Nielsen, S. M.; Bernath, P. F., in preparation.

(5) Alkemade, C. Th. J.; Hollander, Tj.; Snelleman, W.; Zeegers, P. J. Th. *Metal Vapours in Flames*; Pergamon: Oxford, 1982.

(6) Herschel, J. F. W. *Trans. Roy. Soc. Edinburgh* **1823**, *9*, 445–460.

(7) James, C. G.; Sugden, T. M. *Nature (London)* **1955**, *175*, 333–334.

(8) Brom, J. M., Jr.; Weltner, W., Jr. *J. Chem. Phys.* **1976**, *64*, 3894–3895.

(9) Brom, J. M., Jr.; Weltner, W., Jr. *J. Chem. Phys.* **1973**, *58*, 5322–5330.

(10) Harris, D. O., personal communication.

(11) Kauffman, J. M.; Hauge, R. H.; Margrave, J. L. *High Temp. Sci.* **1984**, *18*, 97–118.